Desalination 387 (2016) 61–74

Contents lists available at ScienceDirect

Desalination

journal homepage: www.elsevier.com/locate/desal

How can osmosis and solute diffusion be coupled for the simultaneous measurement of the solvent and solute permeabilities of membranes?

Gustavo H. Lopes [1], Nelson Ibaseta, Pierrette Guichardon *

Aix Marseille Université, CNRS, Centrale Marseille, M2P2 UMR 7340, Pôle de l'Étoile, Technopôle de Château-Gombert, 38 rue Frédéric Joliot-Curie, 13451 Marseille, France

HIGHLIGHTS

- A novel method measures the membrane solvent and solute permeabilities concurrently.
- The method's underlying model is entirely based on osmosis and solute diffusion.
- Osmosis should not be neglected in the calculation of the solute permeability.
- Water and salt permeabilities depend to a large extent on the solution concentration.
- Salt permeabilities thus determined were able to simulate experimental RO rejections.

GRAPHICAL ABSTRACT

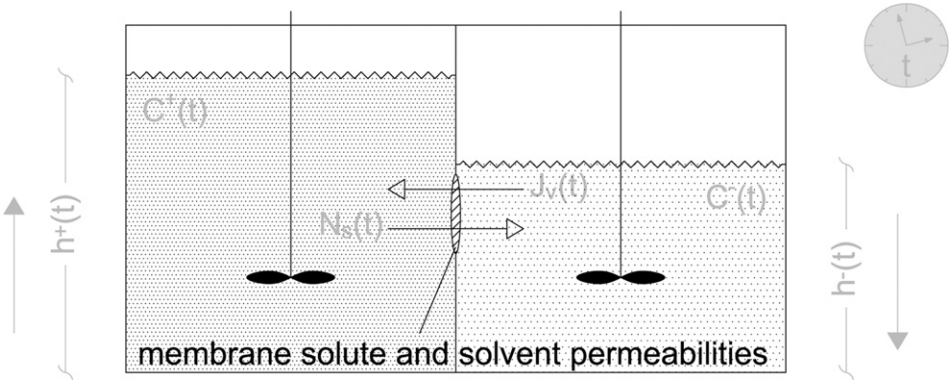

ARTICLE INFO

Article history:
Received 16 November 2015
Received in revised form 2 March 2016
Accepted 5 March 2016
Available online 19 March 2016

Keywords:
Permeability
Osmosis
Reverse osmosis
Rejection rate
Solution–diffusion

ABSTRACT

A novel experimental method and its associated model are proposed for the simultaneous determination of membrane solute and solvent permeabilities, which are essential transport parameters of reverse osmosis models used for process simulation. The method utilizes a single bench-scale batch apparatus consisting of two stirred half-cells containing solutions of different concentrations separated by a membrane across which coupled non-steady-state solute diffusion and solvent osmosis take place countercurrently in the absence of transmembrane pressure difference. Results are presented from days-long determinations of the water and sodium chloride permeabilities of Filmtec BW30 and NF270 membrane samples for initial transmembrane salt concentration differences ranging from 1 g L^{-1} to 35 g L^{-1}. When used as input parameters for the simulation of pilot reverse osmosis desalination tests, the osmotic-diffusive salt permeabilities approximated the experimental rejection rates.

1. Introduction

The development of semipermeable membranes has transformed the way some of the world's most critical issues can be addressed, as for instance water desalination [1–3], water and wastewater treatment [2–5] and sustainable energy generation [6,7]. Several processes based on nonporous osmotic membranes are nowadays viable. These include well-developed industrial processes such as reverse osmosis (RO) [8,

* Corresponding author.
E-mail addresses: gustavo.lopes@centrale-marseille.fr (G.H. Lopes), nelson.ibaseta@centrale-marseille.fr (N. Ibaseta), pierrette.guichardon@centrale-marseille.fr (P. Guichardon).
[1] Present address: Universidad de Ingeniería y Tecnología (UTEC), Jirón Medrano Silva 165, Barranco, Lima, Peru.

http://dx.doi.org/10.1016/j.desal.2016.03.006
0011-9164/

9] as well as other processes under different stages of development, e.g. forward osmosis (FO) [3] and pressure-retarded osmosis (PRO) [7]. For a given set of operating conditions, the productivity and separation efficiency of these processes are functions of the membrane permeabilities to solutes and solvents essentially.

The membrane solute and solvent permeabilities are key input parameters of membrane separation and process models. Knowing them is thus a prerequisite for process performance simulation. In a previous work [10,11] the authors have developed a numerical model of proven appropriateness for reverse osmosis separations in flat geometries. The model is intended to be a readily usable simulation tool with predictive capabilities, using the fewest and simplest input parameters possible. The membrane solvent and solute permeabilities are two of these input parameters.

Permeability measurements may be fraught with biases. When the determinations are performed during pressure-driven filtrations [3, 7–10,12–25], the concentration polarization (CP) phenomenon [10,11] brings uncertainty to the actual concentration difference between the membrane sides. Indeed, quantifying the unstirred concentration boundary layer of non-permeated solutes on the membrane-liquid interface is not trivial. When the permeability measurements are carried out in a purely diffusive setting (in non-pressurized mode) [9,10,12, 16,17,19,26–38], the main concerns are the propensity for internal concentration polarization (ICP), which entangles the determination of the permeabilities of the selective layer of composite membranes, and the occurrence of a countercurrent transmembrane solvent flux. This flux, which is due to osmosis, affects the estimation of the transmembrane solute flux. As a matter of fact, osmosis is not negligeable unless solutions of very low osmotic pressure are considered. All the more, the permeabilities are pressure-sensitive and concentration-dependent [10,19,20,24,26,39,40] and they are influenced by the membrane conditioning protocol [10,21,39,41]. Despite the fundamental interest and the practical relevance of duly addressing these sources of bias, their discussion is scarce. Here, some of these problems are examined and an experimental alternative to them is put forward.

In this paper, we implemented experimental conditions leading to the more general problem in which countercurrent solute diffusion *and* osmosis coexist. Thus, the membrane solvent and solute permeabilities can be determined simultaneously from a single experiment. The governing equations of a batch system formed by two binary liquid solutions of unequal concentrations separated by a solution–diffusion membrane [8,9,12,26,42] subject to non-steady-state solvent and solute permeation, in the absence of any hydrodynamic flows and of any applied pressure, are presented and solved. Then, a suitable in-house built permeation cell and the associated experimental method are presented. They were applied to the determination of the water and sodium chloride permeabilities of commercial reverse osmosis and nanofiltration membrane samples. The concentration-dependence of the parameters thus measured is evidenced. Finally, the applicability of the permeabilities determined herein as input parameters of a reverse osmosis model was evaluated for the prediction of the overall performance of reverse osmosis pilot desalination tests. The paper's findings are of interest to pressure-driven and osmotically driven processes.

2. Literature review

2.1. Solution-diffusion model

Relying on only two transport parameters, namely the molar solvent and solute permeabilities (A and B respectively), for effectively describing separations by nonporous membranes, the classic solution-diffusion (SD) model is far-reaching in RO, FO and PRO. Accordingly, the solvent and the solute are transferred across the membrane in an uncoupled way. Their relative separation results from their difference of solubility and diffusivity in the membrane material [8,9,12,26,42]. The molar fluxes (N) of solvent (subscript v) and solute (subscript s) are directly proportional to their driving forces, respectively the net difference between the transmembrane hydrodynamic pressure difference (ΔP) and transmembrane osmotic pressure difference ($\Delta\Pi$), and the solute concentration difference (ΔC) between the membrane feed and filtrate sides:

$$N_v = A(\Delta P - \Delta\Pi) \tag{1}$$

$$N_s = B(\Delta C). \tag{2}$$

Alternatively to Eq. (1), the volumetric transmembrane solvent flux, J_v, can be defined as

$$J_v = I^{-1}(\Delta P - \Delta\Pi) \tag{3}$$

from what, by writing $\hat{V}_v$ for the solvent molar volume,

$$I^{-1} = \hat{V}_v A. \tag{4}$$

The van't Hoff's law is a typical osmotic pressure law in the water desalination field:

$$\Pi = iRTC \tag{5}$$

where i designates the number of dissociated ionic or neutral units per unit of solubilized solute ($i = 2$ for NaCl), R the ideal gas constant and T the temperature of the solution.

In the following, we review the experimental methods applied for the determination of the membrane solute and solvent permeabilities.

2.2. Permeability determination in pressure-driven filtration

2.2.1. Solvent permeability

I^{-1} is generally determined with Eq. (3) from the slope of a plot of J_v as a function of ΔP in the course of a "filtration" of pure solvent, i.e., when $\Pi = 0$ [3,7–10,12–23,39–41]. Such tests are also performed when new membrane samples are conditioned prior to their end-use in order to remove preservatives [41] and to allow for membrane compaction [39,40] and porosity changes [20], which all cause flux and selectivity modifications. However, standardized conditioning procedures are uncommon [39,41]. Moreover, it is difficult to correlate the operating conditions of the conditioning phase (e.g. the maximal applied pressure and the duration) with the operating conditions set for the membrane's end-use.

2.2.2. Solute permeability

The solute permeability is also mostly determined in the course of some pressure-driven crossflow filtration of a feed solution [3,7–10, 13–19,22–25]. For a given set of operating conditions, B may be fitted to linear relations derived from membrane transport models relating it to experimental crossflow filtration data, like the permeate (filtrate) flux and the solute rejection rate, RR. For the SD model [13]:

$$\frac{1}{RR} = \frac{1}{RR_{\Delta P\to\infty}} + \left(\frac{B}{RR_{\Delta P\to\infty}}\right)\frac{1}{J_v} \tag{6}$$

where

$$RR = 1 - \frac{C_l}{C_u} \tag{7}$$

where u and l denote the upstream (feed side) and downstream (permeate side) membrane-liquid interfaces, and $RR_{\Delta P\to\infty}$ is the limiting value attained by RR for very high J_v when $\Delta P \to \infty$. For a perfect SD-membrane, $RR_{\Delta P\to\infty} = 1$. In reality, an asymptotic value in the range 0.9–0.99 for dense membranes (rationalized as σ, the Staverman

reflection coefficient [9,13,43,44]) is well-known experimentally; however, it is often neglected and set to unity. The ratio $B/RR_{\Delta P\to\infty}$ has already been used as a modified permeability coefficient [14] whose physical interpretation is unclear.

Employing Eq. (6) entails the unavoidable complication of reliably quantifying concentration polarization. Indeed, "intrinsic" ("true", "real") rejection rates, which are calculated from the enhanced membrane surface concentrations instead of from the bulk or the feed concentrations, shall be used for C_u in Eq. (7). However, the experimental measurement of CP layers right on the membrane surface is highly intricate and has only been performed in simplified flow configurations [45,46]. Thus, two issues might be taken but neither of them is optimal: neglecting or calculating CP. The former choice results in inaccurate values of B [15] which severely compromise the subsequent simulation of rejection rates [10,11]. The second choice requires choosing an appropriate concentration polarization model. The boundary layer film model [8] is the most frequent choice in this case but it is faced with well-recognized weaknesses [10]. For calculating membrane surface concentrations, the film model depends on application-specific, empirical mass transfer coefficients and correlations; furthermore, it is a poor one-dimensional treatment of a crossflow, which is by nature a two-dimensional problem coupling momentum and mass transfers.

Representing the mass transfer coefficient of the film model by k and the feed (subscript f) concentration by C_f, a rearrangement of the classic expression of the film model, $(C_u - C_l)/(C_f - C_l) = \exp(J_v/k)$, gives

$$\frac{1-RR_f}{RR_f} = \frac{1-RR}{RR}\exp\left(\frac{J_v}{k}\right) \tag{8}$$

where RR_f is the easily accessible "apparent" (also called "observed") rejection rate:

$$RR_f = 1-\frac{C_l}{C_f} \tag{9}$$

Setting $RR_{\Delta P\to\infty} = 1$ in Eq. (6), it comes that $(1 - RR) / RR = B / J_v$. Rearranging Eq. (8),

$$\ln\left(J_v\frac{1-RR_f}{RR_f}\right) = \frac{J_v}{k} + \ln B \tag{10}$$

Hence, B can be estimated from the ordinate-intercept of a plot of $\ln J_v(1 - RR_f) / RR_f$ versus J_v / k fitted to experimental results. This can be done for either various feed velocities (i.e., for various k) at constant permeate flux (i.e., at constant ΔP) or for various permeate fluxes at constant feed velocity [25,47,48], or, still, from single measurements [18,22].

Eqs. (6) and (10) imply that the determination of B be carried out once the pressure-driven filtration will be already taking place. For predictive process modeling and simulation, this situation is ambiguous since a vicious circle originates: the determination of B presupposes estimating CP by some model while the proper calculation of CP presupposes either knowing the permeate concentration (which is function of B), as in the film model, or of B, as in other CP models [10,11,49].

2.3. Permeability determination in purely diffusive operation

In these types of experiment, sometimes termed dialysis or direct osmosis (DO), two half-cells of a permeation cell containing each a solution of different concentration are separated from each other by a membrane of exposed surface area S as illustrated in Fig. 1. No external pressure is applied in neither solution and the hydrostatic pressure difference is controlled in order to be negligible. The solutions may [16,30,31] or may not [17,26,29,32,34,50] recirculate. In the following, the compartments of higher and lower concentration are symbolized by + and − respectively.

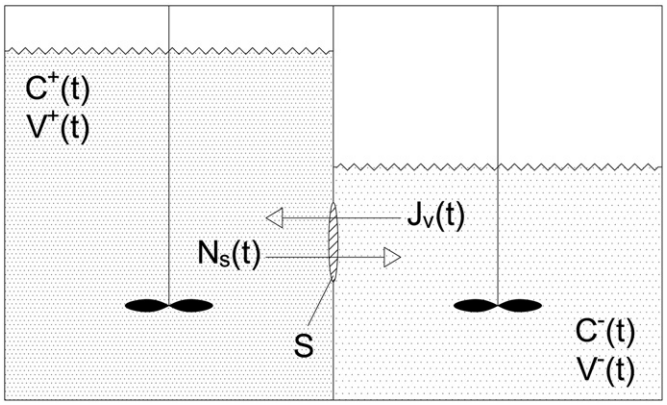

Fig. 1. Schematic diagram of a stirred osmosis-and-diffusion cell whose half-cells are separated by a flat semipermeable membrane of exposed surface area S. The diffusional solute flux across the membrane, N_s, and the solvent osmotic flux, J_v, are proportional to the concentration difference between the concentrated and dilute compartments, $C^+ - C^-$, and have opposite directions. The volumes in each half-cell, V^+ and V^-, are not constant unless osmosis is negligible.

2.3.1. Case of pure solute diffusion

For a system where osmotic pressures are negligible (e.g. for dilute solutions of solutes of low molar mass), only the solute transfer across the membrane from one compartment to the other needs to be considered[2]. B is the only determinable parameter in this case. The volumes of the solutions do not change with time (t) and the solute mass balances in the half-cells read:

$$V^-\left(\frac{dC^-}{dt}\right) = N_sS = B[C^+ - C^-]S \tag{11}$$

$$V^+\left(\frac{dC^+}{dt}\right) = -N_sS = -B[C^+ - C^-]S \tag{12}$$

Dividing Eq. (11) by V^-, Eq. (12) by V^+, subtracting one equation from the other and solving for $C^+ - C^-$, the time evolution of the system is synthesized by the typical relation [51, pp. 23–26; 32]

$$\ln\left(\frac{C_0^+ - C_0^-}{C^+ - C^-}\right) = BS\left(\frac{1}{V^+} + \frac{1}{V^-}\right)t \tag{13}$$

In a convenient experiment, the volumes of each compartment are equal, here noted $V^{\pm}$, and the dilute half-cell is initially solute-free, i.e., $C_0^- = 0$. In these conditions, the solute mass balance in the whole system is:

$$C_0^+V^{\pm} = C^+V^{\pm} + C^-V^{\pm} \tag{14}$$

Combining Eq. (14) with Eq. (13), the following expressions can be obtained [26,29,38]:

$$\ln\left(\frac{C_0^+}{2C^+ - C_0^+}\right) = \left(\frac{2BS}{V^{\pm}}\right)t \tag{15}$$

$$\ln\left(\frac{C_0^+}{C_0^+ - 2C^-}\right) = \left(\frac{2BS}{V^{\pm}}\right)t \tag{16}$$

B can then be obtained with Eqs. (13), (15) or Eq. (16) from the slopes of the plots of the logarithms versus time.

[2] In certain set-ups, the osmotic flux has been kept negligible by compensating the osmotic pressure of the solution containing the solute under study by using, on the other membrane side, a second solution to whose solute the membrane was impermeable [31].

2.3.2. Case of coupled osmosis and solute diffusion

For the more general case where the osmotic solvent flux cannot be neglected, the determination of B via Eqs. (13), (15) or Eq. (16) is inaccurate because the liquid volumes in both half-cells vary with time. Other expressions shall be used; these will then also allow to calculate the solvent permeability from the solvent osmotic flux.

Let the solvent flux be expressed as

$$J_v = \frac{1}{S}\left(\frac{dV^+}{dt}\right) = \frac{-1}{S}\left(\frac{dV^-}{dt}\right) \tag{17}$$

In some DO studies [16,17,30,31,33], regression lines have been fitted on a case-by-case basis to the time evolution of $C^{\pm}$ and/or $V^{\pm}$. These expressions were then differentiated with respect to time, cf. the left-hand side of Eq. (11) or Eq. (12) for the solute, and cf. Eq. (17) for the solvent. Subsequently, the derivatives were injected in Eq. (11) or Eq. (12) (solute), and/or in Eq. (3) (solvent) for $\Delta P = 0$, from whose resulting expressions the permeability values were obtained. It is worth highlighting that this method involves numerical differentiation performed on experimental data, whose accuracy may be a concern [38].

It is remarkable that studies which have determined the solvent permeability under sole a concentration gradient ($\Delta P = 0$) are scarce. For instance, Goosens and Van-Haute [16] have done it and compared the results to values obtained in RO-mode. They observed that the solvent permeabilities I^{-1} in DO were ten times lower than the corresponding RO ones. Matsuda and Kamizawa [31] also verified that the determination of I^{-1} by DO somewhat underestimated water fluxes in RO, but found reasonable agreement; they verified furthermore a little tendency of underestimation when comparing the predictive results calculated using values of B determined in DO to the experimental salt fluxes measured in RO.

2.4. Permeability determination by other methods

In theory, instead of directly measuring I^{-1} and B, permeabilities may still be calculated by separately measuring the membrane thickness, ε, together with the equilibrium partitioning coefficient of a substance in the membrane, K, and the diffusion coefficient of the substance in the membrane, D. As for D_s for instance, salt sorption or desorption experiments can be carried out [12,27]. A membrane is soaked until equilibrium in a solution and subsequently soaked in a pure-water bath; this induces the salt to diffuse out of the membrane at a desorption rate indicative of the salt diffusion coefficient in the membrane. Inversely, the membrane can first be equilibrated in pure solvent and then soaked in a solution bath of known concentration such that solute diffuses into the membrane. If the concentration polarization around the membrane is negligible, the experiment reduces to the classic problem of unsteady-state diffusion in an infinite flat plate with uniform initial profile and negligible surface resistance [52,pp. 461–462]; or, from a mathematical point of view, to a heat equation with Dirichlet conditions [53,chap.2]. If the Fourier series thus obtained is truncated to its first term and then averaged across the membrane for a given time t, Eq. (18) is obtained [8, p. 506; 9,12,27, 52, pp. 461–462]:

$$\frac{\tilde{C}-\tilde{C}_{t\to\infty}}{\tilde{C}_0-\tilde{C}_{t\to\infty}} = \frac{8}{\pi^2}\exp\left(-\frac{\pi^2 D_s}{\varepsilon^2}t\right) \tag{18}$$

where $\tilde{C}$ is the average solute concentration sorbed within the membrane. Then, from the slope of a plot of $\ln[(\tilde{C}-\tilde{C}_{t\to\infty})/(\tilde{C}_0-\tilde{C}_{t\to\infty})]$ as a function of t, it is possible to compute the ratio D_s/ε^2 and, if ε is known, to obtain D_s.

The partitioning coefficient K_s is calculated as the ratio of the steady-state solute equilibrium concentration in the membrane to the solute concentration in the neighboring solution [9,12,17,27,29]. Thermogravimetric analysis, for instance, can be used for quantifying the salt sorbed in membrane films [17]; other methods have been employed too [12,27, 29]. Once these values are known, B can be calculated according to its expression in Eq. (2). However, in addition to analytical inaccuracies when measuring the amount of sorbed or desorbed solute, the knowledge of the membrane thickness, ε, ranging from some nanometers up to a few micrometers, is all but accurate and requires sophisticated experimental techniques [24].

An old study [9] showed that the permeabilities of dense cellulose acetate membranes to sodium chloride in water measured in RO and in DO were more than one order of magnitude higher than those calculated by independently determining D_s and K_s. This points to the existence of some parallel mass transfer mechanism in addition to solution–diffusion (e.g. convective flow) in the former operating modes [9].

Solute permeabilities have also been determined by means of permeation tests with small amounts of radioactive tracer substances and other membrane categories. Tracer permeabilities found with Cuprophan membranes and radiocarbon-labeled sucrose as the solute were significantly lower compared to the phenomenological permeabilities. This is possibly a result of the heterogeneity of the permeation pathways within the membrane [28]. Finally, in recent times, molecular dynamics simulations show encouraging potential for predicting membrane transport properties [8,54].

3. Governing equations

A novel systematic procedure for the determination of membrane solute and solvent permeabilities is proposed from this point on. An isothermal system as that in Fig. 1 is considered. It is composed of two half-cells containing each a binary solution of the same solvent and solute but with different concentrations, separated by a permselective membrane of exposed surface S. The unique driving force in the system is the transmembrane osmotic gradient, i.e., the solute concentration difference across the membrane; no hydraulic or hydrostatic pressure is exerted on neither solution ($\Delta P = 0$). As a result of stirring, the mass transfer resistances in the boundary layers on both membrane sides (CP) are neglected, as well as any buoyancy force leading to natural convection.

Two interdependent, non-steady-state, one-dimensional, antiparallel transmembrane fluxes originate: the solute molar flux N_s *and* the (solvent) volumetric osmotic flux J_v. The latter modifies the volumes in both half-cells, while both fluxes equally determine the concentration changes of both solutions [10,38]. The transmembrane concentration gradient diminishes with time. The van't Hoff's osmotic pressure law is assumed (Eq. (5)). The permeabilities I^{-1} and B are set constant in a same experiment. According to Eqs. (3) and (2) and defining the direction of the solute flux as positive:

$$J_v = -\bar{I}^{-1}\left[C^+ - C^-\right] \tag{19}$$

$$N_s = B\left[C^+ - C^-\right] \tag{20}$$

where

$$\bar{I}^{-1} = iRTI^{-1} \tag{21}$$

It is implied in Eq. (19) that the solute does not contribute to the volume of the solutions and that the hydrostatic pressure created by the difference of liquid levels in the half-cells is negligible compared to $\Delta\Pi$. From Eqs. (19) and (20), the solvent and solute mass balances in the dilute and in the concentrated compartments are, respectively:

$$\frac{1}{S}\left(\frac{dV^-}{dt}\right) = -\bar{I}^{-1}\left[C^+ - C^-\right] \tag{22}$$

$$\frac{1}{S}\left(\frac{dC^-V^-}{dt}\right)=\frac{1}{S}\left(C^-\frac{dV^-}{dt}+V^-\frac{dC^-}{dt}\right)=B\left[C^+-C^-\right] \tag{23}$$

$$\frac{1}{S}\left(\frac{dV^+}{dt}\right)=\bar{I}^{-1}\left[C^+-C^-\right] \tag{24}$$

$$\frac{1}{S}\left(\frac{dC^+V^+}{dt}\right)=\frac{1}{S}\left(C^+\frac{dV^+}{dt}+V^+\frac{dC^+}{dt}\right)=-B\left[C^+-C^-\right] \tag{25}$$

The mass balances from Eqs. (11) and (12) are retrieved for $I^{-1}=0$.

3.1. Calculation of the ratio of permabilities

The evolution of the concentrations and volumes is a function of their initial values and of I^{-1} and B only. Therefore, before solving the systems of equations above, it may be of interest to track the mutual progression of those variables independently of time. Noticing that [10]

$$\frac{dC^\pm}{dV^\pm}=\frac{dC^\pm}{dt}\Big/\frac{dV^\pm}{dt} \tag{26}$$

it follows from Eqs. (22) and (23) or from Eqs. (24) and (25) that

$$\frac{dC^\pm}{dV^\pm}=-\frac{1}{V^\pm}\left(\frac{B}{\bar{I}^{-1}}+C^\pm\right) \tag{27}$$

An opportune experiment would start with pure solvent in the dilute half-cell, so that $C_0^-=0$. In this case, by solving Eq. (27) and rearranging [10]:

$$C^-=\frac{B}{\bar{I}^{-1}}\left(\frac{V_0^-}{V^-}-1\right) \tag{28}$$

$$C^+=\frac{B}{\bar{I}^{-1}}\left(\frac{V_0^+}{V^+}-1\right)+C_0^+\frac{V_0^+}{V^+} \tag{29}$$

Eq. (28) is especially practical for gaining a first insight into the membrane permselectivity via the ratio of permeabilities $B/\bar{I}^{-1}$.

The analogous mathematical development for a membrane following the Kedem–Katchalsky transport model [9,44] is found in the Appendix A.

3.2. Calculation of the solvent and solute permeabilities separately

The mass conservation in the system as a whole is, at any time:

$$V^-+V^+=V_0^-+V_0^+ \tag{30}$$

$$C^-V^-+C^+V^+=C_0^-V_0^-+C_0^+V_0^+ \tag{31}$$

By combining these equations with, for instance, Eqs. (22) and (23), the derivatives of the volume and of the concentration of the dilute solution can be isolated as functions of unknowns of the dilute compartment only. The following system of first-order ordinary differential equations is obtained:

$$\frac{dV^-}{dt}=\bar{I}^{-1}S\left(\frac{C^-V^-}{V_0^++V_0^--V^-}+C^--\frac{C_0^+V_0^++C_0^-V_0^-}{V_0^++V_0^--V^-}\right) \tag{32}$$

$$\frac{dC^-}{dt}=\bar{I}^{-1}S\left(\frac{C^-\left[C_0^+V_0^++C_0^-V_0^-\right]+\left[C^-\right]^2\left[V_0^++V_0^-\right]}{V^-\left[V_0^++V_0^--V^-\right]}\right)+BS\left(\frac{C_0^+V_0^++C_0^-V_0^-+C^-\left[V_0^++V_0^-\right]}{V^-\left[V_0^++V_0^--V^-\right]}\right). \tag{33}$$

Eq. (32) and (33) can be solved with the objective of determining $\bar{I}^{-1}$ and B by fitting these parameters to experimental data of C^- and V^-. This will be done in Section 5.

A similar system could be written for the concentrated solution. Alternatively, the values of C^+ and V^+ can be readily calculated from the mass conservation expressions, Eqs. (30) and (31), after solving Eqs. (32) and (33).

4. Materials and methods

Two types of experiments have been carried out. First, the usual determination of the membrane water permeability in pressure-driven crossflow filtration of pure water (cf. Sections 2.2.1 and 4.2); these experiments are sometimes referred to as “membrane conditioning” in this text. Afterwards, the determination of the membrane water and salt permeabilities under a concentration gradient only (cf. Sections 3 and 4.3) took place.

4.1. Membrane samples

The BW30 and NF270 commercial flat-sheet polyamide thin-film composite (TFC) membrane samples manufactured by Dow Filmtec (USA) were employed. In pressure-driven applications, the former is a brackish-water RO membrane and the latter is a loose-NF membrane for high rejection of organics but capable of only partial softening and low salt rejection. Since the membrane structure and mass transfer mechanisms inside NF membranes are markedly distinct from those of an RO membrane, the results obtained with the NF270 in this study are only meant to be a comparison with those obtained with the BW30 for similar initial conditions.

4.2. Membrane conditioning

The SEPA CF II (GE Osmonics, USA) bench-scale plate-and-frame crossflow filtration unit was used. It accommodated a membrane with an effective filtration area of 132 cm^2 and whose selective layer was always facing the feed stream. Ultrapure water was fed into the flow channel at 298 ± 1 K at the desired transmembrane pressure with a circulation velocity of 0.8 m s^{-1}. The permeate of each experiment was weighted in a collection vessel by an analytical balance (Precisa XT 4200C, Switzerland) connected to a data acquisition program set with a measurement time step of 5 s. More details on the equipment can be found elsewhere [10].

For each membrane, the conditioning cycle lasted for about 2.5 h. During an initial “cleaning” stage of 10 min, ΔP was maintained practically at zero and no permeate flux was detected. It was then increased by 5- to 10-min-long increments up to approximately 25×10^5 Pa, maintained at this plateau for 1 h and eventually brought back to zero by increments. The membrane samples have not undergone any other treatment. The maximal conditioning pressure is low in comparison with typical operating pressures in seawater desalination. However, it corresponds with the operating pressures used during the pilot experiments (Section 5.3.1). It is also in agreement with the characteristic operating pressures in brackish water desalination.

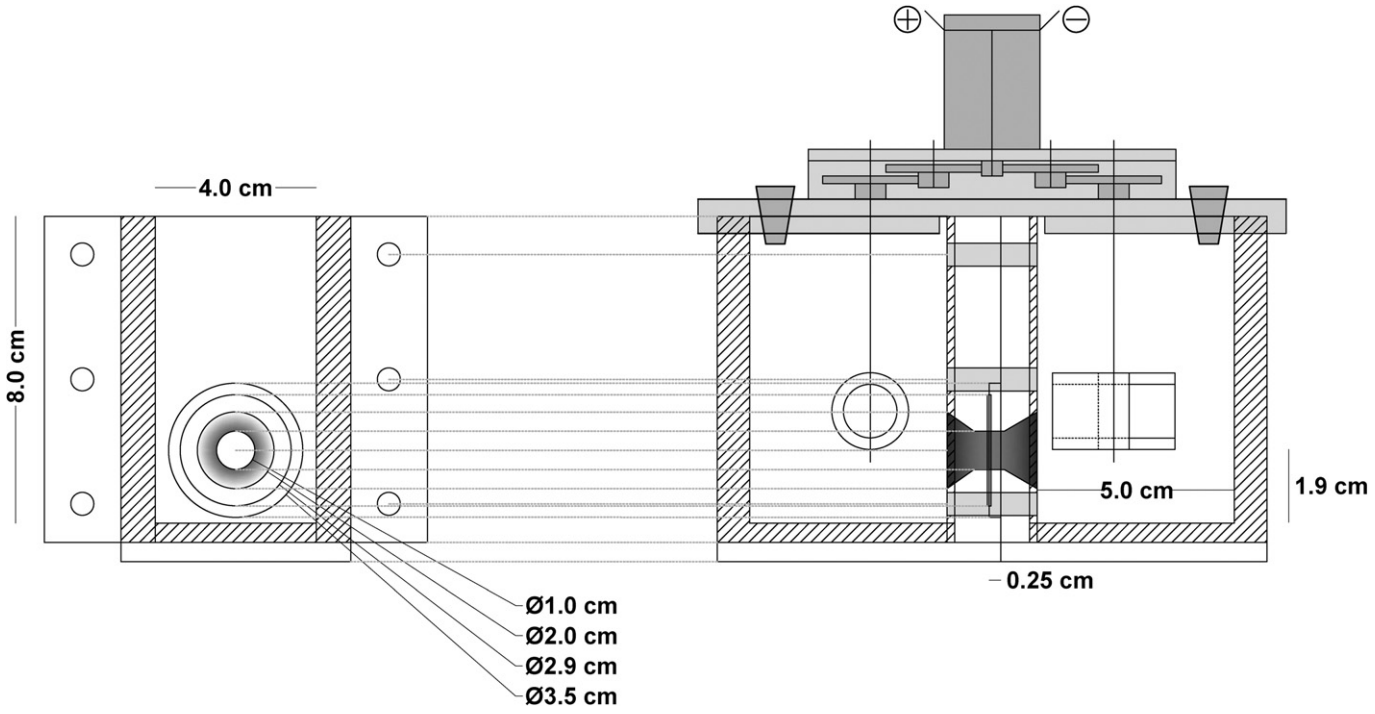

Fig. 2. Schematic representation of the stirred batch permeation cell used for the determination of the membrane permeabilities via osmosis and solute diffusion. On the left-hand side, front view of a half-cell seen in the direction parallel to the membrane. On the right-hand side, front view of the experimental set-up assembled with the half-cells face-to-face and shown in the direction perpendicular to the membrane surface.

4.3. Determination of the water and salt permeabilities via osmotic-diffusive experiments

The stirred permeation cell represented in Fig. 2 was used. It is a batch device composed of two half-cells made of acrylic. Each half-cell is 8.0 cm high on the inner side and has a 5.0 cm × 4.0 cm inner cross-sectional area for an effective capacity of 160 mL. Both have a vertical aperture in symmetrical positions drilled, depending on the half-cell, either in a thin horizontal cylindrical prominence or in the corresponding thin hollow. These apertures limit the effective membrane area exposed to the solutions to $S = 0.785\ \mathrm{cm}^2$. Once the half-cells are assembled face-to-face and fastened tightly against each other, a nozzle-shaped channel, with the membrane in its middle, extends from the inner side of a half-cell's wall up to the inner side of the other half-cell's wall. A lid prevented contamination and evaporation and housed the gear system of the electrically driven stirring mechanism. Stirring speed was fixed at 120 rpm. The experimental set-up was checked for the absence of communicating vessels before each experiment. No pump, valve or recirculation system is used. Further descriptions are presented in [10].

An experiment started by filling the half-cells simultaneously: in the concentrated compartment, approximately 100 mL of a sodium chloride (reagent grade, Honeywell Seelze, Germany) solution prepared with distilled water; in the dilute chamber, approximately 100 mL of pure distilled water (exact values in Table 1). The membrane's selective layer was always in contact with the concentrated solution. As shown in Table 1, ten experiments in total have been done, 5 with a same BW30 sample and 5 with a same NF270 sample, and 3 initial salt concentration differences typical of water desalination applications have been tested: 1, 10 and 35 g L^{-1} (17.1, 171.1 and 598.9 mol m^{-3}). The durations of the experiments – from 5 to 15 days – were functions of the measurability of the evolution of the concentration in the dilute half-cell (where the measurements were more sensitive) and of the height of liquid (h) in the compartments (in order to prevent overflow in the concentrated side and to ensure that the membrane was always submerged in the dilute side). For the same reasons, measurements were done either one or a few times a day at most. A blank test carried out with distilled water during 8 days resulted in only 1.7% volume loss by evaporation in each half-cell.

The liquid levels (without stirrers) were measured with a graduated ruler. The concentration and temperature of both solutions were measured with a conductivity meter (Eutech/Oakton CON 11, Singapore/USA) equipped with a built-in temperature sensor (EC-CONSEN91W 35608–50); minor losses of solution occurred after each measurement in both half-cells when wiping the conductivity electrode dry. The measurements were performed systematically first in the dilute compartment and only after in the concentrated half-cell; the meter's electrode was rinsed and wiped dry before and after each of these measurements.

Table 1
Overview of all osmotic-diffusive experiments carried out, their initial conditions and their labels as adopted in this paper. C_0^+, C_0^-, V_0^+ and V_0^- are, respectively, the initial sodium chloride concentrations and initial volumes of the concentrated and dilute aqueous solutions. The initial concentrations of the concentrated salt solutions on the second column of the table were of 1 g L^{-1}, 10 g L^{-1} and 35 g L^{-1}; the values in these units are mnemonically integrated into the experiments' labels.

Membrane sample	C_0^+ (mol m^{-3})	C_0^- (mol m^{-3})	V_0^+ m^3	V_0^- m^3	Experiment's label
BW30 (RO)	17.1	0	9.9×10^{-5}	9.9×10^{-5}	B1A
			9.9×10^{-5}	1.0×10^{-4}	B1B
	171.1	0	9.7×10^{-5}	9.7×10^{-5}	B10A
	598.9	0	9.6×10^{-5}	9.6×10^{-5}	B35A
			1.0×10^{-4}	1.0×10^{-4}	B35B
NF270 (NF)	17.1	0	9.8×10^{-5}	9.8×10^{-5}	N1A
			9.7×10^{-5}	9.9×10^{-5}	N1B
	171.1	0	9.6×10^{-5}	9.6×10^{-5}	N10A
			9.8×10^{-5}	9.9×10^{-5}	N10B
	598.9	0	9.9×10^{-5}	9.9×10^{-5}	N35A

Table 2
Water permeability of the RO and NF membrane samples in pressure-driven crossflow filtration of pure water (membrane conditioning phase).

Membrane	l^{-1} (m Pa^{-1} s^{-1})
BW30 (RO)	8.74 (±0.04) 10^{-12}
NF270 (NF)	5.72 (±0.01) 10^{-11}

5. Results and discussions

5.1. Membrane conditioning

The final water permeability values of the conditioned membranes *under an applied transmembrane pressure* are listed in Table 2. Not surprisingly, the water permeability of the reverse osmosis membrane was much lower than that of the nanofiltration membrane.

As mentioned in Section 2.2.1, pressure-induced mechanical compaction and porosity modifications are known to influence the membrane mass transfer properties. Indeed, for both membrane samples, the permeability evolved considerably with ΔP during the increasing-pressure cycle of the conditioning protocol, but kept a constant value throughout the subsequent decreasing-pressure cycle [10].

5.2. Osmotic-diffusive experiments

Henceforth, calculations are based on measurements and other data relative to the dilute half-cell only since the conductivity measurements in this compartment were more sensitive.

5.2.1. Measurements of osmosis and salt diffusion

Let V_{osm} be the total "accumulative" volume of water transferred by osmosis from the dilute compartment ("water reservoir") into the concentrated half-cell, and m_{diff} be the mass of NaCl which diffused from the concentrated half-cell ("salt reservoir") into the dilute compartment:

$$V_{osm} = LW\left[h^{-} - h_0^{-}\right] - V_{loss} \tag{34}$$

$$m_{diff} = LW\left[C^{-}h^{-} - C_0^{-}h_0^{-}\right]M_s - m_{loss}^{-} \tag{35}$$

where $L = 0.05$ m and $W = 0.04$ m (in the current set-up), and V_{loss} and m_{loss}^{-} are small terms explained in the Appendix B accounting for minor water and salt losses.

Fig. 3 presents the ratios between the total volume of water transferred by osmosis, V_{osm}, and the initial volume of the dilute half-cell, V_0^{-}, as a function of the elapsed time. It can be seen that the osmotic effect is higher with the BW30, a membrane typically more selective

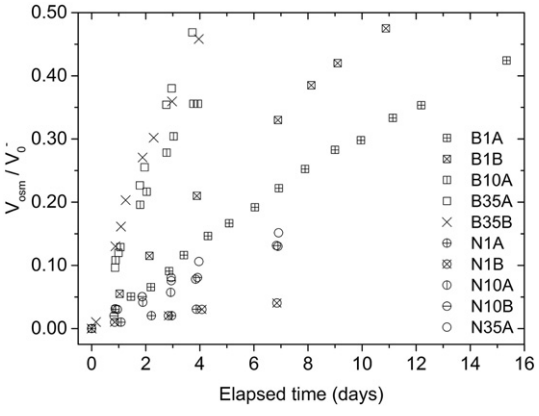

Fig. 3. Fraction of the water of the dilute half-cell drawn with time by osmosis for all experiments.

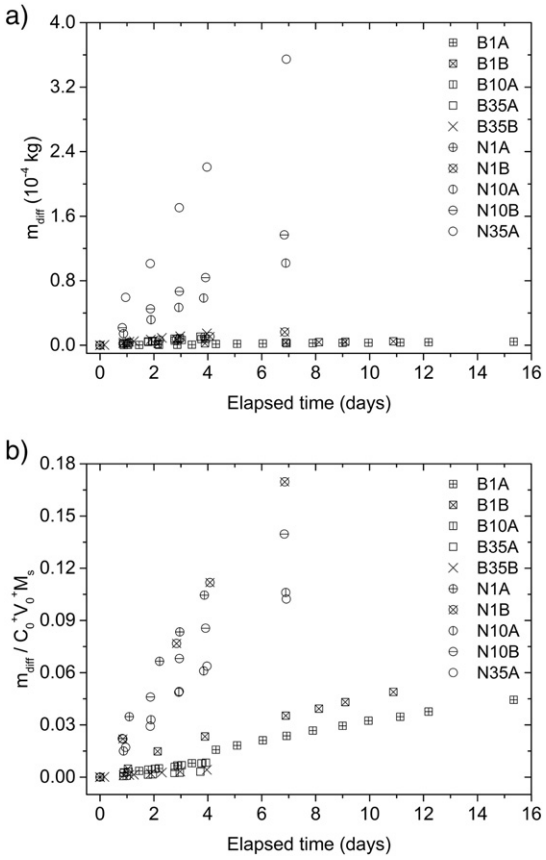

Fig. 4. For all experiments, (a) absolute mass of salt which diffused into the dilute half-cell and (b) mass of salt which diffused into the dilute half-cell compared to the initial mass of salt in the concentrated half-cell.

than NF membranes in pressure-driven filtration. When comparing m_{diff} for both membranes in Fig. 4a, the solute transfer is higher for the NF270, the less selective of the two in pressure-driven operation. Still, when considering in Fig. 4b the ratio between m_{diff} and the initial amount of salt in the salt reservoir (C_0^+), it can be seen that this ratio decreased for higher C_0^+. This is the same as saying that this ratio decreased for higher concentration differences between the two compartments, since the concentration in the concentrated solution was always much higher than that in the dilute solution [10]. Hence, it is already possible to infer from Fig. 4b that the membrane salt permeability (B) decreased with increasing salt concentration for both membranes tested. Finally, since the plots are very close to straight lines, it is reasonable to assume that the membrane permeabilities were constant along the duration of a same experiment.

For illustration, Fig. 5 presents the instant measurements of the heights, solute concentrations and temperatures of the concentrated and dilute solutions in the course of the osmotic-diffusive experiment B10A. The measurements carried out during the other experiments are presented in reference [10].

5.2.2. Water and salt permeabilities

Fig. 6 illustrates, with the experiment B10A, the linear regressions fitted to the experimental data of $V_0^{-}/V^{-} - 1$ as a function of C^{-} (as in Eq. (28) but with the position of the axes modified). These values have been previously corrected by taking into account the eventual losses, as explained in Appendix B. The fittings for all other experiments can be found in [10].

The fourth, fifth and sixth columns of Table 3 contain the permeability ratios B/l^{-1} determined according to Eq. (28) for all experiments.

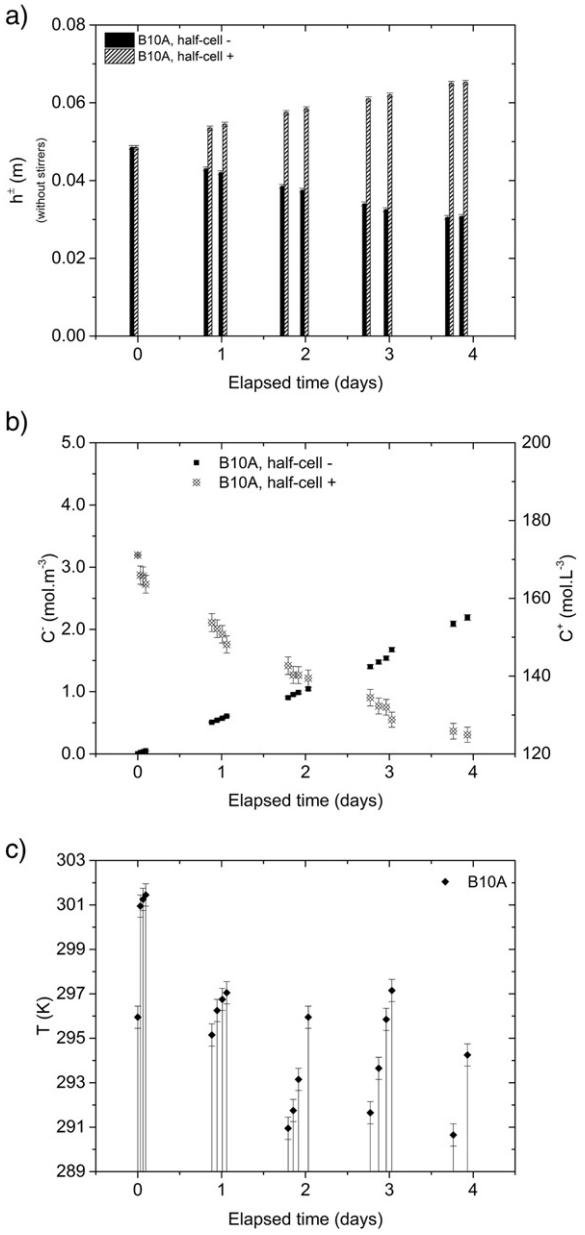

Fig. 5. Evolution of the (a) liquid column heights, (b) salt concentrations and (c) temperatures measured along several days in the concentrated (+) and dilute (−) half-cells illustrated for the experiment of osmosis and diffusion B10A.

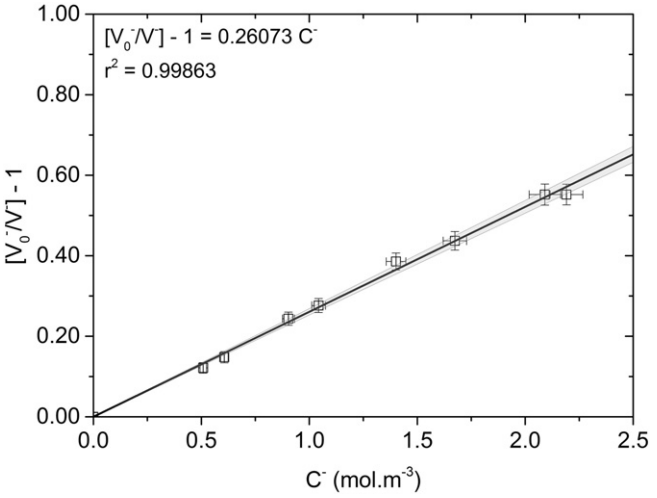

Fig. 6. Mutual time-evolution of $V_0^-/V^- - 1$ and C^- for the experiment B10A. Lower and upper 95%-confidence intervals calculated with the software OriginPro 9.1 for the ordinate-error weighted least square straight line are shown in light gray in the plot; r^2 is the coefficient of determination of the fitted line. From the reciprocal of the slope of this plot, the ratio of permeabilities $B/\bar{I}^{-1}$ can be calculated from Eq. (28) and, hence, B/I^{-1} can be determined (see Table 3).

The order of magnitude of $B/\bar{I}^{-1}$ for the two membranes is completely different: 1 mol m^{-3} for the BW30 and 10^1 mol m^{-3} or 10^2 mol m^{-3} for the NF270. Furthermore, the values are clearly concentration-dependent: as $\Delta C_0 = C_0^+ - C_0^-$ increases by a factor 10 or by a factor 35 for the BW30 and the NF270, the ratios practically double or triple for the former membrane and increase by approximately 2–3 times or by 6 times for the NF270 respectively. The results for experiments B1B and B1A coincide. They differ of 23% when comparing B35B to B35A (same magnitude although no overlap in the confidence intervals); of 8% when comparing N1B to N1A (overlap in the confidence intervals) and of 21% when comparing N10B to N10A (same magnitude although no overlap in the confidence intervals).

The evolutions of the corrected values of C^- and V^- are presented in Fig. 7 together with the plots generated by solving Eqs. (32) and (33) fitting simultaneously the unknowns I^{-1} and B to the experimental data (notice that V^- is little sensitive to B). A fourth-order Runge–Kutta scheme [55,p. 897] with a fixed time step of 5 min has been implemented in the program Microsoft Excel 2010 for this purpose. The results obtained for the two membranes are grouped in Fig. 8 and transcribed in the seventh and eighth columns of Table 3. The ninth column of Table 3 shows that the ratio of permeabilities calculated with the fitted permeabilities are similar to the ratios of permeability obtained directly from the least-square straight lines, what confirms the validity of both approaches.

As can be seen in Fig. 8 and in Table 3, the water and salt permeabilities decreased significantly with the initial transmembrane concentration difference in osmotic-diffusive operation. The concentration-dependence of the water permeability was even stronger: I^{-1} of the RO and NF membrane samples decreased up to one order of magnitude when ΔC_0 changed from 17.1 mol m^{-3} to 598.9 mol m^{-3}; meanwhile, the reduction of B varied between 3 and 6 times for the RO sample and 1.7 times for the NF sample. The decrease of permeabilities with the increase of the solute concentration is qualitatively in agreement with the free volume theory of diffusion in polymers [26,29,35] and could also be related to the modification of the equilibrium partitioning constants (solute and solvent contents of the membrane) and to osmotic swelling/shrinkage of the membrane material [9,35]. As for I^{-1} still, it was evidenced that the solvent permeability in osmotic-diffusive operation was much lower than that under pressure in 9 of 10 experiments: up to one order of magnitude for the BW30 and to two orders of magnitude for the NF270. The experimental reproducibility was mostly good for I^{-1} (5% relative difference between B35B and B35A, equality between N1B and N1A and 11% difference between N10B and N10A), except for the experiments B1B and B1A (41%). It was mostly poor for B (38% relative difference between B1B and B1A, 21% between B35B and B35A and 32% between N10B and N10A), except for the experiments NF1A and NF1B (5%). No satisfactory explanation has been found for the non-reproducibility of experiments. Differences in the average temperature during repeated experiments, the possibility of occurrence of small surface defects when the membrane samples were handled, or, still, the modification of CP conditions due to eventual oscillations in the functioning of the stirrers might be factors behind this finding.

For illustration, the errors incurred by the use of Eq. (16), originally deduced for the determination of the solute permeability in a situation of negligible osmotic flux, can be calculated at this point with the data in Table 3. Not surprisingly, the agreements between the salt permeabilities calculated via Eq. (16) and via the numerical fitting to the solution

Table 3

Synthesis of all values of salt and water permeability, B and I^{-1} respectively, and of selectivity, B/I^{-1}, obtained from the osmotic-diffusive experiments. From Eq. (21), $\overline{I}^{-1} = iRTI^{-1}$ where $i = 2$ and $T = 293$ K. LCL and UCL: least-square straight line's lower and upper confidence limits. The initial salt concentration differences on the second column were of 1 g L^{-1}, 10 g L^{-1} and 35 g L^{-1}.

Membrane	ΔC_0 (mol m^{-3})	Experiment	From Eq. (28)			From Eqs. (32) and (33) and Fig. 7		
			$B/\overline{I}^{-1}$ (mol m^{-3})			B (m s^{-1})	I^{-1} (m Pa^{-1} s^{-1})	$B/\overline{I}^{-1}$ (mol m^{-3})
			LCL	Mean value	UCL			
BW30 (RO)	17.1	B1A	1.7	1.8	1.9	5.6×10^{-8}	6.5×10^{-12}	1.8
		B1B	1.7	1.8	1.9	9.0×10^{-8}	1.1×10^{-11}	1.7
	171.1	B10A	3.7	3.8	4.0	3.6×10^{-8}	2.1×10^{-12}	3.5
	598.9	B35A	3.8	4.0	4.1	1.5×10^{-8}	7.0×10^{-13}	4.4
		B35B	4.8	5.2	5.6	1.9×10^{-8}	7.4×10^{-13}	5.3
	17.1	N1A	54.3	60.9	69.2	4.6×10^{-7}	1.5×10^{-12}	62.9
		N1B	57.8	66.3	77.9	4.4×10^{-7}	1.5×10^{-12}	60.2
NF270 (NF)	171.1	N10A	124.7	137.3	152.7	2.6×10^{-7}	4.0×10^{-13}	133.4
		N10B	160.0	173.1	188.5	3.8×10^{-7}	4.5×10^{-13}	173.3
	598.9	N35A	356.3	381.7	411.0	2.6×10^{-7}	1.5×10^{-13}	355.8

of the system of Eqs. (32) and (33) were close only in the cases were V^{-1} varied little (NF membrane). When the volume of the solutions varied significantly (RO membrane), the errors incurred ranged from 27% up to 45% [10]. This confirms the inadequacy of the classic Eq. (16) for determining permeabilities in the general case of non-negligible osmotic pressures [10,38].

It is also of primary importance to highlight the discrepancies between the salt permeabilities determined by numerical fitting to the solution of the system of Eqs. (32) and (33) and the salt permeability values which one would be assuming if an osmotic-diffusive ratio of permeabilities were combined with a water permeability determined in pressure-driven crossflow filtration. The comparisons are shown in Table 4. Salt permeabilities 2 to 3 orders of magnitude above the actual ones would be found for the NF membrane and up to 1 order of magnitude for the RO membrane. In other words, the membrane selectivity in these experiments was not conserved between situations where the membrane undergoes a pressure or a concentration (osmotic pressure) difference.

Finally, an unconventional finding was that the water permeabilities (and water fluxes) determined in osmosis and salt diffusion were in most cases much higher for the RO membrane than for the NF membrane, what is the opposite of the results typically found in pressure-driven filtration. It is not likely that setting the Staverman reflection coefficient to unity when modeling the solvent flux in Eq. (19) (i.e., that writing I^{-1} instead of σI^{-1} [9,44]), be behind this finding; this would mean that σ for the NF270 needs to be of order 10^{-2}–10^{-1} for its permeability to be of a similar or higher magnitude than that of the BW30. Such values are too low for σ, especially in the absence of ΔP. Again, the fundamental inequality between $\Delta\Pi$ and ΔP as regards the mass transfer mechanisms that they engendered across the TFC membranes is put in evidence and points, seemingly, to a significant contribution of ΔP-induced convective flow as a parallel transfer mechanism.

5.3. Simulation of reverse osmosis

Our final goal is to evaluate the usefulness of the osmotic-diffusive permeability values as input parameters of predictive models for reverse osmosis.

5.3.1. Rejection rates in reverse osmosis

In order to compare the salt permeabilities determined herein with those which fit the values of apparent rejection rate measured in RO with membranes of the same specification, pilot experiments described elsewhere [10,11,56] have been performed in a spiral-wound module equipped with a BW30-4040 membrane (Dow Filmtec, USA) with aqueous sodium chloride solutions of concentrations similar to the values of ΔC_0 tested in osmotic-diffusive mode. In a previous work [10,11], the authors have proposed a numerical model which considers the coupling of membrane transport to hydrodynamics and bulk (i.e., across the polarization concentration layer) mass transfer. In this model, the membrane permeabilities intervene in the boundary conditions of the flow domain. The values of the solute permeability B have then been fitted, aiming to reproduce the experimental rejection rates RR_f.

Even though these rates were not exactly fitted by the salt permeabilities determined in osmosis and diffusion, these values of B were still very useful since they yielded right magnitudes of RR_f; for many operating conditions at lower feed concentration all the more, a very close agreement was found. As shown in Fig. 9a for the RO experiment with a feed solution of 1.4 g L^{-1} and in Fig. 9b for a feed solution of 10.0 g L^{-1}, a unique permeability value was capable of satisfactorily fitting the rejection rates obtained for different operating pressures/permeate fluxes for a same concentration. Indeed, as formalized by the classic solution-diffusion model, the solute transmembrane chemical potential gradient, which is the driving force for solute transfer across the membrane, is essentially insensitive to pressure [8,9]. This is implied in Eq. (2), where the pressure-dependent term $-\hat{V}_s\Delta P/RT$ is neglected [8] and the only remaining effect of pressure is due to its very slight influence on the diffusion and partitioning coefficients of the solute. The concentration-dependence of B is observed in pressure-driven operation [11].

Some dissimilarities between the osmotic-diffusive experiments and the pressure-driven tests with the spiral-wound module deserve to be highlighted: the fact that the membranes used in both cases are not the same single samples though they have the same specifications; the difference between the maximal operating pressures used during the conditioning of the two RO membranes (25×10^5 Pa with the flat sample and 22×10^5 Pa with the spiral-wound membrane); the variation of the temperature during the osmotic-diffusive experiments versus the constancy of the feed temperature during the RO tests. Also, each membrane sheet in the spiral-wound module measures approximately 0.88 m^2 whereas the sample used for the osmotic-diffusive tests had a surface area of only 0.785 cm^2: it is known that spatial variation of values of solvent and solute permeabilities can exist along a same membrane sheet due to manufacturing reasons [21]. Finally, studies with spiral-wound modules in PRO have suggested that tensile stresses generated in the membrane material undergoing deformation caused by the feed spacer subject to pressure influence the membrane permeabilities and selectivity to water and salt [22].

That said, the results emphasize the applicability of the osmotic-diffusive determination of the solute permeability as an integral part of a predictive approach for the simulation of rejection rates of reverse osmosis processes.

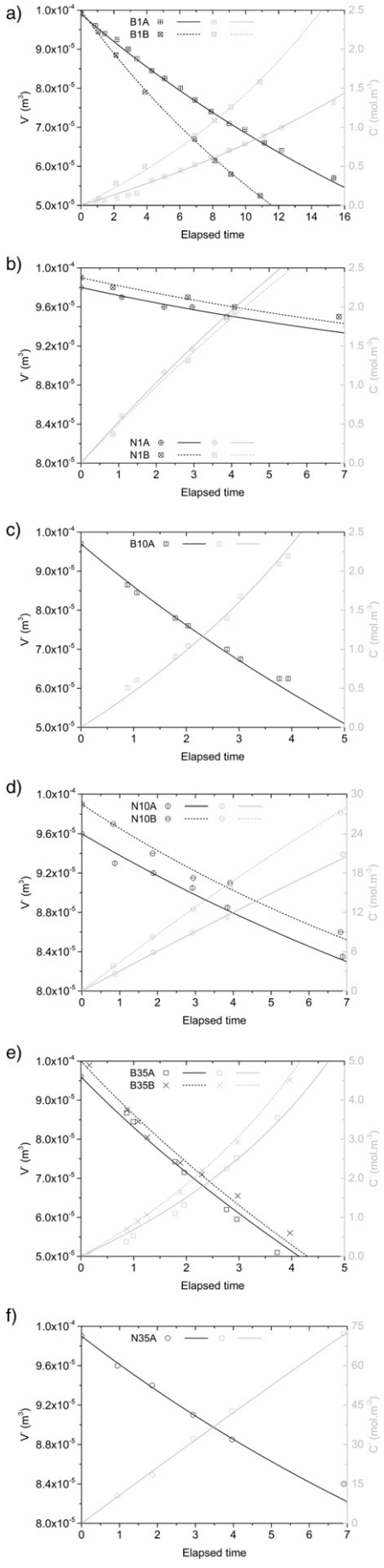

5.3.2. Permeate fluxes in reverse osmosis

The RO-permeate fluxes of this work are insensitive to B because the permeate obtained with membranes of so low salt permeability is very dilute.

Most water permeabilities determined for the RO membrane sample in osmosis-and-diffusion (Table 3) are up to one order of magnitude lower than that determined under pressure (Table 2) and that of the spiral-wound membrane (Fig. 9). As a consequence, the use of the osmotic permeabilities for the simulation of the RO permeate fluxes totally underestimates the fluxes.

The membranes used in this study have an anisotropic structure. Their ultra-thin selective layers lie on reinforcement porous substrates [8,9] across which a non-negligible mass transfer resistance exists when purely diffusion-induced transmembrane transfer takes place. This occurrence is termed internal concentration polarization (ICP) in the literature of osmotically driven processes [3,7,18,23,37,38]. ICP must be contributing to the fact that the osmotic water permeabilities determined herein are much lower than those measured under pressure during the membrane conditioning, but it is sound to extend the discussion beyond this phenomenon. For instance, permeability changes engendered by the development of mechanical stresses (internal pressure gradients) in the membrane material subject to pressure could also be put forward [19,57] – this topic goes largely unstudied in the membrane field.

It is also worth mentioning that the "exchange" of coefficients among essentially different membrane-solution states, as is the case of systems under pressure or under osmotic gradients, has been questioned by a few authors [10,19,36,37]. Care shall be therefore exercised when establishing quantitative links between permeabilities in RO, FO and PRO applications. Attention should also be paid to the concentration-dependence of the permeabilities for the three processes at usual water desalination conditions and to the influence of the membrane conditioning pressure on the membrane transport properties.

6. Conclusions

A model and an experimental method for the simultaneous determination of both solute and solvent membrane permeabilities are proposed. The values which are thus obtained have a reasonable accuracy and enable the predictive simulation of pilot reverse-osmosis experiments. The experimental set-up is simple and only small amounts of solution and small membrane surfaces are necessary, making the method interesting despite the duration of the experiments.

An improvement for the experimental set-up is the addition of a device which maintains the temperature of the solutions at a constant value. The present set-up only measures the temperature but does not control it, reason why temperature differences of approximately 10 K occurred during a same experiment. Therefore, some physical properties (mainly viscosity and diffusion coefficients) fluctuated during the experiments. The order of magnitude of the permeabilities should be considered for such experiments rather than the exact numerical values. In spite of that, the temperature control pertains to the experimental device and does not cast doubt on neither the method nor the model that are proposed.

Osmotic-diffusive membrane water permeabilities were found to be lower than the membrane water permeabilities under hydrodynamic pressure by several orders of magnitude. Therefore, at present, the

Fig. 7. Plots of the experimental results (dots) of volume and concentration of the dilute half-cell and of the corresponding numerical solutions (lines) of Eqs. (32) and (33) generated by parametric fitting of I^{-1} and B to the experimental data.

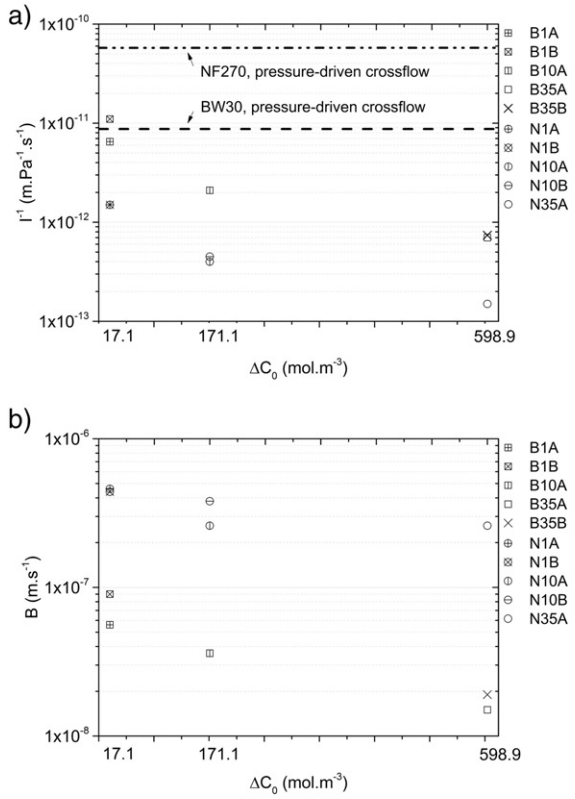

Fig. 8. Membrane permeabilities determined either via osmosis-and-diffusion for initial transmembrane salt concentration differences of 1 g L^{-1}, 10 g L^{-1} and 35 g L^{-1} or determined during pressure-driven pure-water crossflow filtration. (a) Water permeabilities. (b) Salt permeabilities.

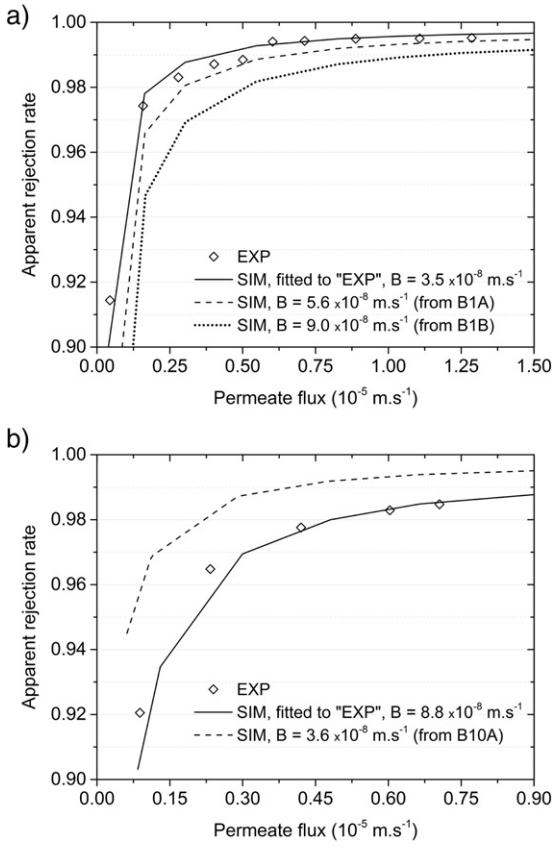

Fig. 9. Experimental (dots) and simulated (lines) rejection rates as functions of the permeate fluxes during the RO desalination of model aqueous sodium chloride solutions of concentration (a) 24.0 mol m^{-3} (1.4 g L^{-1}) and (b) 171.1 mol m^{-3} (10.0 g L^{-1}) with the BW30–4040 spiral-wound membrane module. The values of salt permeability obtained during the osmotic-diffusive experiments with the BW30 are inputs for the simulations (dashed lines). The RO experiments have been carried out at 298 ± 1 K with inlet pressures ranging from 1×10^5 Pa to 20.5×10^5 Pa and an inlet circulation velocity of 0.11 m s^{-1} (feed Reynolds number of 212). The water permeability of the BW30–4040 membrane determined previously in pressure-driven crossflow with pure water was 7.13×10^{-12} m Pa^{-1} s^{-1}, thus a little below the 8.74×10^{-12} m Pa^{-1} s^{-1} found for the flat BW30 sample in Table 2. Simulations reproduced the intense mixing in the flow channel by employing an effective Schmidt number [10,11,56] of 50.

determination of the solvent permeability for RO purposes must be done under pressure-driven pure-solvent filtration as usually. These findings indicate a dissimilarity between the water transport mechanisms engendered by pressure and by osmotic pressure (concentration) differences across composite (anisotropic) membranes. Further studies with isotropic membranes would be insightful. The novel method is appropriate for the determination of the value of membrane solute permeability when osmosis is not negligible since it properly considers the effect of the countercurrent solvent osmotic flux on the calculations.

Table 4
Discrepancies between the purely osmotic-diffusive sodium chloride permeabilities fitted to the numerical solution of Eqs. (32) and (33) in Fig. 7 and those, hypothetical, which would be assumed if water permeabilities determined in pressure-driven pure-water crossflow filtration (Table 2) were assigned to the osmotic-diffusive ratios of permeability calculated with Eq. (28).

Experiment	Pure osmotic-diffusive mode	Osmotic-diffusive $B/\bar{I}^{-1}$ mixed with the pressure-driven I^{-1}
	B (m s^{-1})	
B1A	5.6×10^{-8}	7.5×10^{-8}
B1B	9.0×10^{-8}	7.4×10^{-8}
B10A	3.6×10^{-8}	1.6×10^{-7}
B35A	1.5×10^{-8}	1.7×10^{-7}
B35B	1.9×10^{-8}	2.1×10^{-7}
N1A	4.6×10^{-7}	1.7×10^{-5}
N1B	4.4×10^{-7}	1.8×10^{-5}
N10A	2.6×10^{-7}	3.8×10^{-5}
N10B	3.8×10^{-7}	4.8×10^{-5}
N35A	2.6×10^{-7}	1.0×10^{-4}

The classic solution-diffusion model has been considered here. Other membrane transport models which seek a more fundamental comprehension and accurate quantification of the small-scale mass transfer across the membranes may also be combined with the method here developed. Extracting their numerous transport parameters by means of the experiments here proposed is yet to be assessed.

Nomenclature and units

Greek symbols
Δ [−] transmembrane difference
ε [m] membrane thickness
Π [Pa] osmotic pressure
σ [−] Staverman reflection coefficient
ω [mol m^{-2} Pa^{-1} s^{-1}]
molar Kedem-Katchalsky membrane solute permeability

Latin symbols
A [mol m^{-2} Pa^{-1} s^{-1}]
molar solution-diffusion membrane solvent permeability
B [m s^{-1}] molar solution-diffusion membrane solute permeability

C [mol m^{-3}]
solute concentration
D [m^2 s^{-1}]
diffusion coefficient
h [m] height of solution in the half-cell
i [−] van't Hoff's solute dissociation factor
I [Pa s m^{-1}]
membrane resistance to transmembrane volumetric solvent flux (its reciprocal is the volumetric membrane solvent permeability)
J [m^3 m^{-2} s^{-1}], [m s^{-1}] volumetric flux
k [m s^{-1}] mass transfer coefficient
K [−] equilibrium partitioning coefficient
L [m] inner length of the half-cell (direction perpendicular to the membrane)
m [kg] mass of solute
M [kg mol^{-1}] molar mass
N [mol m^{-2} s^{-1}] molar flux
P [Pa] hydrodynamic pressure
r^2 [−] coefficient of determination of a regression line
R [m^3 Pa K^{-1} mol^{-1}] ideal gas constant
RR [−] solute rejection rate
S [m^2] area
t [s] elapsed time
T [K] temperature
V [m^3] volume
W [m] inner width of the half-cell (direction parallel to the membrane)

Other symbols
$\mathcal{L}$ [m Pa^{-1} s^{-1}]
volumetric Kedem-Katchalsky membrane solvent permeability

Sub- and superscripts
app apparent or effective
corrected value corrected for losses
diff diffused
f feed solution
l permeate-side membrane-liquid interface
loss amount lost
osm transferred by osmosis
s solute
u feed-side membrane-liquid interface
v solvent
$\hat{}$ molar property
$\hat{}$ average transmembrane value
$\tilde{}$ value within the membrane
$\bar{}$ value multiplied by *iRT*
± reference to the concentrated or dilute solutions/half-cells
+ reference to the concentrated solution/half-cell
- reference to the dilute solution/half-cell
∞ infinite

Abbreviations
CP concentration polarization
DO direct osmosis
EXP experimental value
FO forward osmosis
ICP internal concentration polarization
NF nanofiltration
PRO pressure-retarded osmosis
RO reverse osmosis
SD solution-diffusion
SIM simulated value
TFC thin-film composite

Acknowledgments

The authors thank Prof. Olivier Boiron and Dr. Yannick Knapp (Institut de Recherche sur les Phénomènes Hors Équilibre, Marseille, France) as well as Dr. Marie-Pierre Belleville (Institut Européen des Membranes, Montpellier, France) and Mr. Alain Kilidjian (École Centrale de Marseille) for their material support, and Prof. Pierre Haldenwang (Laboratoire de Mécanique, Modélisation et Procédés Propres, Marseille, France) for enriching discussions.

This work was funded by the Conseil Régional Provence-Alpes-Côte d'Azur and the École Centrale de Marseille.

Appendix A. Expressions for a Kedem-Katchalsky membrane

In the Kedem-Katchalsky membrane transport model, solute and solvent transports are coupled via the Staverman reflection coefficient σ ($0 \le \sigma \le 1$) [9,13,19,43,44]. This parameter reflects the degree of semi-permeability of a leaking membrane, i.e., its propensity for transporting across itself the solvent rather than the solute. The solvent and solute fluxes in a purely concentration-driven operation read:

$$J_v = -\sigma\overline{\mathcal{L}}\left[C^+ - C^-\right] \tag{A.1}$$

$$N_s = \overline{\omega}\left[C^+ - C^-\right] + (1-\sigma)\hat{C}J_v \tag{A.2}$$

where

$$\overline{\mathcal{L}} = iRT\mathcal{L} \tag{A.3}$$

and

$$\overline{\omega} = iRT\omega \tag{A.4}$$

The solvent and solute mass balances for the dilute half-cell are [10]:

$$\frac{dV^-}{dt} = -\sigma\overline{\mathcal{L}}S\left[C^+ - C^-\right] \tag{A.5}$$

$$C^- \frac{dV^-}{dt} + V^- \frac{dC^-}{dt} = \overline{\omega}S\left[C^+ - C^-\right] - (1-\sigma)\hat{C}\sigma\overline{\mathcal{L}}S\left[C^+ - C^-\right] \tag{A.6}$$

From what it is possible to write [10]:

$$\frac{dC^-}{dV^-} = -\left(\frac{\overline{\omega}}{\sigma\overline{\mathcal{L}}} + \sigma\hat{C} + \left[C^- - \hat{C}\right]\right)\frac{1}{V^-} \tag{A.7}$$

Considering that $\hat{C}$ is roughly constant and that $C_0^- = 0$ [10]:

$$C^- = \left[\frac{\overline{\omega}}{\overline{\mathcal{L}}}\right]_{app}\left(\frac{V_0^-}{V^-} - 1\right) \tag{A.8}$$

where

$$\left[\frac{\overline{\omega}}{\overline{\mathcal{L}}}\right]_{app} = \left(\frac{\overline{\omega}}{\sigma\overline{\mathcal{L}}} - (1-\sigma)\hat{C}\right) \tag{A.9}$$

The subscript *app* stands for "apparent" or effective.

In comparison with the expressions for a solution-diffusion membrane, two more parameters need to be known or determined in addition to the permeabilities: σ and $\hat{C}$. The latter is an approximation of $\hat{C}$ often took as the logarithmic mean of the solute concentrations on the two membrane-liquid sides [13].

Appendix B. Expressions for correcting volumes and concentrations for losses

Considering that liquid losses by evaporation and during wiping of the conductivity electrode are similar in both half-cells during the osmotic-diffusive experiments, and assuming that losses due to possible (but unlikely) leaks are equally distributed between the two membrane sides, the volume lost in a half-cell until time t may be written:

$$V_{loss} = \frac{V_0^- + V_0^+ - V^- - V^+}{2} \tag{B.1}$$

$$m_{loss}^- = \left[C^- - C_0^-\right] V_{loss} M_s \tag{B.2}$$

By writing $C^- - C_0^-$ instead of, for instance, $[C^- - C_0^-]/2$, a conservative estimate for m_{loss}^- is obtained from Eq. (B.2). The volume and concentration in the dilute half-cell corrected for losses may then be written:

$$V_{corrected}^- = V^- + V_{loss} \tag{B.3}$$

$$C_{corrected}^- = \frac{C^- V^- + m_{loss}^- M_s^{-1}}{V^-} \tag{B.4}$$

The volume losses at the end of the experiments were below 5% of the initial volume of the dilute half-cell in most cases, except for the experiment B35B during which a leak was detected in the concentrated half-cell (approximately 13% of the initial volume of the dilute half-cell). The salt losses were 2 to 3 orders of magnitude lower than the salt mass that diffused into the dilute compartment. The formulas above are therefore presented for the sake of generality, and the corrections for losses had only minor influence on the final permeability values.

References

[1] C. Charcosset, A review of membrane processes and renewable energies for desalination, Desalination 245 (2009) 214–231, http://dx.doi.org/10.1016/j.desal.2008.06.020.

[2] W.L. Ang, A. Wahab Mohammad, N. Hilal, C.P. Leo, A review on the applicability of integrated/hybrid membrane processes in water treatment and desalination plants, Desalination 363 (2015) 2–18, http://dx.doi.org/10.1016/j.desal.2014.03.008.

[3] T.Y. Cath, A.E. Childress, M. Elimelech, Forward osmosis: principles, applications, and recent developments, J. Membr. Sci. 281 (2006) 70–87, http://dx.doi.org/10.1016/j.memsci.2006.05.048.

[4] M. Raffin, E. Germain, S. Judd, Wastewater polishing using membrane technology: a review of existing installations, Environ. Technol. 34 (2013) 617–627, http://dx.doi.org/10.1080/09593330.2012.710385.

[5] K. Lutchmiah, A.R.D. Verliefde, K. Roest, L.C. Rietveld, E.R. Cornelissen, Forward osmosis for application in wastewater treatment: a review, Water Res. 58 (2014) 179–197, http://dx.doi.org/10.1016/j.watres.2014.03.045.

[6] B.E. Logan, M. Elimelech, Membrane-based processes for sustainable power generation using water, Nature 488 (2012) 313–319, http://dx.doi.org/10.1038/nature11477.

[7] K.L. Lee, R.W. Baker, H.K. Lonsdale, Membranes for power generation by pressure-retarded osmosis, J. Membr. Sci. 8 (1981) 141–171, http://dx.doi.org/10.1016/S0376-7388(00)82088-8.

[8] R.W. Baker, Membrane Technology and Applications, third ed. John Wiley & Sons, Chichester, United Kingdom, 2012.

[9] M. Soltanieh, W.N. Gill, Review of reverse osmosis membranes and transport models, Chem. Eng. Commun. 12 (1981) 279–363, http://dx.doi.org/10.1080/00986448108910843.

[10] G.H. Lopes, On the Coupling of Membrane Transport to Hydrodynamics and Bulk Mass Transfer in Reverse Osmosis: Numerical Modeling and Experimental Studies Ph.D., thesis École Centrale de Marseille, 2014.

[11] G.H. Lopes, N. Ibaseta, P. Guichardon, P. Haldenwang, Predicting permeate fluxes and rejection rates in reverse osmosis and tight-nanofiltration processes, Chem. Eng. Technol. 38 (2015) 585–594, http://dx.doi.org/10.1002/ceat.201400654.

[12] H.K. Lonsdale, U. Merten, R.L. Riley, Transport properties of cellulose acetate osmotic membranes, J. Appl. Polym. Sci. 9 (1965) 1341–1362, http://dx.doi.org/10.1002/app.1965.070090413.

[13] W. Pusch, Determination of transport parameters of synthetic membranes by hyperfiltration experiments part I: derivation of transport relationship from the linear relations of thermodynamics of irreversible processes, Ber. Bunsenges. Phys. Chem. 81 (1977) 269–276, http://dx.doi.org/10.1002/bbpc.19770810306.

[14] P. Lipp, R. Gimbel, F.H. Frimmel, Parameters influencing the rejection properties of FT30 membranes, J. Membr. Sci. 95 (1994) 185–197, http://dx.doi.org/10.1016/0376-7388(94)00124-3.

[15] W. Zhou, L. Song, Experimental study of water and salt fluxes through reverse osmosis membranes, Environ. Sci. Technol. 39 (2005) 3382–3387, http://dx.doi.org/10.1021/es0403561.

[16] I. Goosens, A. Van-Haute, The use of direct osmosis tests as complementary experiments to determine the water and salt permeabilities of reinforced cellulose acetate membranes, Desalination 26 (1978) 299–308, http://dx.doi.org/10.1016/S0011-9164(00)82204-3.

[17] L.-Y. Hung, S. Jessie Lue, J.-H. You, Mass-transfer modeling of reverse-osmosis performance on 0.52% salty water, Desalination 265 (2011) 67–73, http://dx.doi.org/10.1016/j.desal.2010.07.033.

[18] T.Y. Cath, M. Elimelech, J.R. McCutcheon, R.L. McGinnis, A. Achilli, D. Anastasio, A.R. Brady, A.E. Childress, I.V. Farr, N.T. Hancock, J. Lampi, L.D. Nghiem, M. Xie, N. Yin Yip, Standard methodology for evaluating membrane performance in osmotically driven membrane processes, Desalination 312 (2013) 31–38, http://dx.doi.org/10.1016/j.desal.2012.07.005.

[19] W. Pusch, Chapter 1.4 Measurement techniques of transport through membranes, Desalination 59 (1986) 105–198, http://dx.doi.org/10.1016/0011-9164(86)90028-7.

[20] K. Košutić, L. Kaštelan-Kunst, B. Kunst, Porosity of some commercial reverse osmosis and nanofiltration polyamide thin-film composite membranes, J. Membr. Sci. 168 (2000) 101–108, http://dx.doi.org/10.1016/S0376-7388(99)00309-9.

[21] T. Schipolowski, A. Jeżowska, G. Wozny, Reliability of membrane test cell measurements, Desalination 189 (2006) 71–80, http://dx.doi.org/10.1016/j.desal.2005.06.014.

[22] Q. She, D. Hou, J. Liu, K.H. Tan, C.Y. Tang, Effect of feed spacer induced membrane deformation on the performance of pressure retarded osmosis (PRO): implications for PRO process operation, J. Membr. Sci. 445 (2013) 170–182, http://dx.doi.org/10.1016/j.memsci.2013.05.061.

[23] S.S. Manickam, J.R. McCutcheon, Model thin film composite membranes for forward osmosis: demonstrating the inaccuracy of existing structural parameter models, J. Membr. Sci. 483 (2015) 70–74, http://dx.doi.org/10.1016/j.memsci.2015.01.017.

[24] E. Dražević, K. Košutić, V. Freger, Permeability and selectivity of reverse osmosis membranes: correlation to swelling revisited, Water Res. 49 (2014) 444–452, http://dx.doi.org/10.1016/j.watres.2013.10.029.

[25] G. Jonsson, C.E. Boesen, Concentration polarization in a reverse osmosis test cell, Desalination 21 (1977) 1–10, http://dx.doi.org/10.1016/S0011-9164(00)84104-1.

[26] G.M. Geise, B.D. Freeman, D.R. Paul, Sodium chloride diffusion in sulfonated polymers for membrane applications, J. Membr. Sci. 427 (2013) 186–196, http://dx.doi.org/10.1016/j.memsci.2012.09.029.

[27] M.A. Frommer, J.S. Murday, R.M. Messalem, Solubility and diffusivity of water and of salts in an aromatic polyamide film, Eur. Polym. J. 9 (1973) 367–373, http://dx.doi.org/10.1016/0014-3057(73)90096-7.

[28] R.A. Meyer, E.C. Hills, M.H. Friedman, Tracer permeabilities underestimate transmembrane solute flux under a concentration gradient, J. Membr. Sci. 8 (1981) 247–253, http://dx.doi.org/10.1016/S0376-7388(00)82313-3.

[29] H. Yasuda, C.E. Lamaze, L.D. Ikenberry, Permeability of solutes through hydrated polymer membranes. Part I. Diffusion of sodium chloride, Makromol. Chem. 118 (1968) 19–35, http://dx.doi.org/10.1002/macp.1968.021180102.

[30] S.M.S. Ghiu, R.P. Carnahan, M. Barger, Permeability of electrolytes through a flat RO membrane in a direct osmosis study, Desalination 144 (2002) 387–392, http://dx.doi.org/10.1016/S0011-9164(02)00348-X.

[31] M. Matsuda, C. Kamizawa, Precise measurement of membrane constants of cellulose acetate membranes by direct osmosis tests, Desalination 49 (1984) 367–378, http://dx.doi.org/10.1016/0011-9164(84)85044-4.

[32] B. Falk, S. Garramone, S. Shivkumar, Diffusion coefficient of paracetamol in a chitosan hydrogel, Mater. Lett. 58 (2004) 3261–3265, http://dx.doi.org/10.1016/j.matlet.2004.05.072.

[33] G. Jonsson, J. Benavente, Determination of some transport coefficients for the skin and porous layer of a composite membrane, J. Membr. Sci. 69 (1992) 29–42, http://dx.doi.org/10.1016/0376-7388(92)80165-G.

[34] E.P. Honig, J.H.T. Hengst, Permeation through $BaSO_4$-precipitate membranes, Electrochim. Acta 17 (1972) 75–90, http://dx.doi.org/10.1016/0013-4686(72)85009-6.

[35] G.M. Geise, D.R. Paul, B.D. Freeman, Fundamental water and salt transport properties of polymeric materials, Prog. Polym. Sci. 39 (2014) 1–42, http://dx.doi.org/10.1016/j.progpolymsci.2013.07.001.

[36] A. Zelman, R. Tankersley, A. Ford, H. Wayt, A. Schindler, The membrane transport matrix: analytical and experimental techniques for complete characterization, J. Electrochem. Soc. 123 (1976) 1015–1023, http://dx.doi.org/10.1149/1.2132983.

[37] A. Tiraferri, N. Yin Yip, A.P. Straub, S. Romero-Vargas Castrillon, M. Elimelech, A method for the simultaneous determination of transport and structural parameters of forward osmosis membranes, J. Membr. Sci. 444 (2013) 523–538, http://dx.doi.org/10.1016/j.memsci.2013.05.023.

[38] A. Yaroshchuk, Influence of osmosis on the diffusion from concentrated solutions through composite/asymmetric membranes: theoretical analysis, J. Membr. Sci. 355 (2010) 98–103, http://dx.doi.org/10.1016/j.memsci.2010.03.013.

[39] Y.A. Hussain, M.H. Al-Saleh, A viscoelastic-based model for TFC membranes flux reduction during compaction, Desalination 344 (2014) 362–370, http://dx.doi.org/10.1016/j.desal.2014.04.010.

[40] Y.A. Hussain, M.H. Al-Saleh, S.S. Ar-Ratrout, The effect of active layer non-uniformity on the flux and compaction of TFC membranes, Desalination 328 (2013) 17–23, http://dx.doi.org/10.1016/j.desal.2013.08.008.

[41] S. Wright, J. Pellegrino, G. Amy, Humectant release from membrane materials, J. Membr. Sci. 246 (2005) 227–234, http://dx.doi.org/10.1016/j.memsci.2004.07.030.
[42] D.R. Paul, Reformulation of the solution–diffusion theory of reverse osmosis, J. Membr. Sci. 241 (2004) 371–386, http://dx.doi.org/10.1016/j.memsci.2004.05.026.
[43] A.J. Staverman, The theory of measurement of osmotic pressure, Recueil Trav. Chim. Pays-Bas 70 (1951) 344–352, http://dx.doi.org/10.1002/recl.19510700409.
[44] O. Kedem, A. Katchalsky, Thermodynamic analysis of the permeability of biological membranes to non-electrolytes, Biochim. Biophys. Acta 27 (1958) 229–246, http://dx.doi.org/10.1016/0006-3002(58)90330-5.
[45] J.C. Chen, Q. Li, M. Elimelech, In situ monitoring techniques for concentration polarization and fouling phenomena in membrane filtration, Adv. Colloid Interf. Sci. 107 (2004) 83–108, http://dx.doi.org/10.1016/j.cis.2003.10.018.
[46] C. Rodrigues, P. Garcia-Algado, V. Semião, M.N. de Pinho, V. Geraldes, Concentration boundary layer visualization in nanofiltration by holographic interferometry with light deflection correction, J. Membr. Sci. 447 (2013) 306–314, http://dx.doi.org/10.1016/j.memsci.2013.07.035.
[47] Z.V.P. Murthy, S.K. Gupta, Estimation of mass transfer coefficient using a combined nonlinear membrane transport and film theory model, Desalination 109 (1997) 39–49, http://dx.doi.org/10.1016/S0011-9164(97)00051-9.
[48] I. Sutzkover, D. Hasson, R. Semiat, Simple technique for measuring the concentration polarization level in a reverse osmosis system, Desalination 131 (2000) 117–127, http://dx.doi.org/10.1016/S0011-9164(00)90012-2.
[49] E. Nagy, E. Kulcsár, A. Nagy, Membrane mass transport by nanofiltration: coupled effect of the polarization and membrane layers, J. Membr. Sci. 368 (2011) 215–222, http://dx.doi.org/10.1016/j.memsci.2010.11.046.
[50] T.M.B. Teodósio, T.S. Cavallini, L.V. Jardim, G.J.-F. Demets, Montagem de uma célula universal para ensaios de permeação em membranas semipermeáveis sólidas em escala laboratorial, Orbital 3 (4) (2011) 204–211.
[51] E.L. Cussler, Diffusion: Mass Transfer in Fluid Systems, third ed. Cambridge University Press, Cambridge, United Kingdom, 2009.
[52] C.J. Geankoplis, Transport Processes and Separation Process Principles (Includes Unit Operations), fourth ed. Prentice Hall, Upper Saddle River, United States, 2003.
[53] R. Haberman, Elementary Applied Partial Differential Equations, third ed. Prentice Hall, Upper Saddle River, United States, 1998.
[54] Y. Luo, E. Harder, R.S. Faibish, B. Roux, Computer simulations of water flux and salt permeability of the reverse osmosis FT-30 aromatic polyamide membrane, J. Membr. Sci. 384 (2011) 1–9, http://dx.doi.org/10.1016/j.memsci.2011.08.057.
[55] P.J. Davis, I. Polonsky, Numerical Interpolation, Differentiation, and Integration, in: M. Abramowitz, I.A. Stegun (Eds.), Handbook of Mathematical Functions with Formulas, Graphs, and Mathematical Tables, June 1964's Issue, 10th Printing, United States Department of Commerce, National Bureau of Standards, December 1972.
[56] G.H. Lopes, P. Guichardon, N. Ibaseta, P. Haldenwang, L'eau, ressource rare? Gros plan sur le procédé de dessalement par membranes d'osmose inverse, Actual. Chim. 390 (2014) 85–87.
[57] N. Kocherginsky, Mass transport and membrane separations: universal description in terms of physicochemical potential and Einstein's mobility, Chem. Eng. Sci. 65 (2010) 1474–1489, http://dx.doi.org/10.1016/j.ces.2009.10.024.